A Comparative Study on the Thermoelectric Performance of Layered β- and ε-GaSe

Wenyan Jiao(焦文艳), HongmeiYuan(袁红梅), Shihao Han(韩世豪), Yufeng Luo(罗宇峰), Haibin Cao(曹海斌), and Huijun Liu(刘惠军)*

Key Laboratory of Artificial Micro- and Nano-Structures of Ministry of Education and School of Physics and Technology, Wuhan University, Wuhan 430072, China

(Received 22 March 2025; accepted manuscript online 20 June 2025)

Due to the weak interlayer interactions, the binary Ⅲ-Ⅵ chalcogenides GaSe can exist in several distinct polymorphs. Among them, the so-called β- and ε-phases simultaneously exhibit favorable total energies and moderate band gaps, which offer a good platform to explore their thermoelectric properties. Here, we demonstrate by first-principles calculations that the two systems have very similar band structures and phonon dispersions, despite different stacking sequences between adjacent layers. Interestingly, the lattice thermal conductivity of ε-GaSe is obviously lower than that of β-GaSe, which is inherently tied to stronger lattice anharmonicity caused by bonding heterogeneity. Besides, both systems exhibit higher p-type power factors due to doubly degenerate bands with weaker dispersions around the valence band maximum. As a consequence, a significantly enhanced p-type figure-of-merit of 2.1 can be realized at 700 K along the out-of-plane direction of the ε-phase.

DOI: 10.1088/0256-307X/42/8/080603 CSTR: 32039.14.0256-307X.42.8.080603

1. Introduction. Thermoelectric (TE) materials exhibit remarkable capability of directly converting heat into electricity, providing an alternative way to overcome the increasingly serious energy crisis and environmental pollution. The TE conversion efficiency of a given system is usually determined by the dimensionless figure-of-merit, $ZT = S^2\sigma T/(\kappa_e + \kappa_l)$. Here, S is the Seebeck coefficient, σ is the electrical conductivity, T is the absolute temperature, and κ_l (κ_e) is the lattice (electronic) thermal conductivity. Owing to the complex inter-coupling of these transport coefficients, it is usually very challenging to simultaneously achieve a higher power factor ($PF = S^2\sigma$) and a lower thermal conductivity. To improve the TE performance of a given material, many novel strategies have been proposed to decouple the transport coefficients, such as band structure engineering,[1–3] nanostructure designing,[4] high-entropy alloying,[5] and so on. Among the rapidly growing class of TE materials, layered systems have attracted extensive attention, benefiting from their unique crystal structure characterized by strong intralayer bonds but weak interlayer interactions.[6–11] Such a strong discrepancy in bonding strength is expected to result in partially localized low-frequency phonon modes, low sound velocities, and large anharmonicities, which are all favorable for achieving a low lattice thermal conductivity.[12–15] Furthermore, layered materials usually exhibit anisotropic electron and phonon transport, offering the potential to decouple intercorrelated TE coefficients. For example, the Bi_2Te_3-based materials display higher ZT along the in-plane direction, primarily due to their superior higher mobility,[16] despite also having a higher intralayer κ_l than that along the out-of-plane direction. In contrast, compared with that along the in-plane direction, the $SnSe_2$[17] and SnSe compounds[18,19] show higher ZT along the cross-plane direction, which is mainly attributed to their significantly lower interlayer κ_l. A similar picture was also observed in the Zintl phase BaAgSb.[20] Furthermore, the Mg_3Sb_2 single crystal exhibits a larger ZT value along the out-of-plane direction, owing to its simultaneously lower κ_l and higher cross-plane carrier mobility.[21] All these findings highlight the critical influence of anisotropic transport behavior on optimizing the TE efficiency in layered materials.

Recently, the layered Ⅲ-Ⅵ chalcogenides GaSe have been subjected to intensive investigation,[22–26] which are composed of vertically stacked Se-Ga-Ga-Se layers held together by relatively weak van der Waals (vdW) forces. Such systems can be found in several polytypes, as characterized by different stacking sequences.[27–29] By adopting density functional theory (DFT) calculations, Al-Hattab *et al.*[30] predicted that the semiconducting β-, ε-, δ-, and γ-GaSe exhibit direct band gaps of 0.818 eV, 0.751 eV, 0.888 eV, and 0.819 eV, respectively. Among them, the β- and ε-phases belong to the hexagonal system consisting of eight atoms, and the former has an inversion center. Meanwhile, Magorrian *et al.*[31] found that these two systems simultaneously exhibit favorable energies and moderate band gaps. On the other hand, Nissimagoudar *et al.*[32] reported that in monolayer group 13 monochalcogenides GaSe, each Se atom has a tetrahedral configuration due to the sp^3 hybridization, whereas three of the four hybridized orbitals form the Ga-Se bonds, and the remaining one is

*Corresponding author. Email: phlhj@whu.edu.cn

© 2025 Chinese Physical Society and IOP Publishing Ltd. All rights, including for text and data mining, AI training, and similar technologies, are reserved.

fully occupied by lone pair electrons. Such a characteristic is favorable for increasing the phonon anharmonicity and thus reduces the lattice thermal conductivity. Despite significant interest in the structural and electronic properties, there is still a lack of theoretical predictions on the thermoelectric transport properties of layered GaSe, such as the Seebeck coefficient, the electrical conductivity, the thermal conductivity, and the figure of merit.

In this work, the thermoelectric properties of β- and ε-GaSe compounds are comparatively explored by first-principles calculations combined with Boltzmann theory. It is interesting to discover that the β- and ε-phase exhibit very similar electronic transport properties and phonon dispersion relations. Surprisingly, the lattice thermal conductivities of these two structures are quite different, as governed by their distinct bonding heterogeneity. In particular, the ε-GaSe exhibits a larger anharmonicity and thus smaller lattice thermal conductivity. As a consequence, a maximum ZT value of 2.1 can be achieved for the ε-GaSe at an intermediate temperature of 700 K.

2. Computational Method. Within the framework of DFT, the electronic properties of the layered β- and ε-GaSe are calculated by using the plane-wave pseudopotential method, as performed in the Vienna *ab initio* simulation package (VASP).[33] The exchange-correlation functional is in the form of Perdew–Burke–Ernzerhof with the generalized gradient approximation.[34] A carefully tested $19 \times 19 \times 3$ Monkhorst-Pack k-mesh is used for sampling the Brillouin zone, and the cutoff energy for the plane-wave expansion is set as 500 eV. The system is fully relaxed until the magnitude of the residual force acting on each atom is less than 0.01 eV·Å^{-1} and the energy convergence criteria is 10^{-6} eV. The long-range vdW interactions between adjacent layers are treated by adopting the widely recognized DFT-D3 functional,[35] and spin–orbit coupling is explicitly considered in the calculations. On top of the band structure, we adopt the Boltzmann transport theory[36] to derive the electronic transport coefficients S, σ, and κ_e, where the carrier relaxation time τ can be accurately evaluated by considering scattering from all the phonon modes. For simplicity, the electron–phonon coupling matrix is regarded as a constant, and τ of the n-th band at the wavevector $\boldsymbol{k}$ can be expressed as $\tau^{-1}_{n\boldsymbol{k}} = \frac{2\pi k_B T E^2_{\rm def}}{VG\hbar} \sum_{m\boldsymbol{k}'} \delta(\varepsilon_{n\boldsymbol{k}} - \varepsilon_{m\boldsymbol{k}'})$. Such a treatment is implemented in the TransOpt code,[37] where $E_{\rm def}$, $\varepsilon_{n\boldsymbol{k}}$, V, G, k_B, and $\hbar$ are the deformation potential constant, the energy eigenvalue, the volume of the unit cell, the Young's modulus, the Boltzmann constant, and the reduced Planck constant, respectively. Compared with the simple constant relaxation time approximation or the deformation potential theory, our approach significantly enhances the calculation accuracy without huge computational resources. It should be mentioned that this method has been successfully used to reliably predict the electronic transport properties of many thermoelectric materials.[38–40] For the phonon transport calculations, the second- and third-order interatomic force constants (IFCs) are calculated by utilizing the finite displacement method with a $4 \times 4 \times 2$ supercell, as realized in the Phonopy package[41] and the Thirdorder.py script, respectively. Besides, the seventh nearest neighbors are included for the third-order interactions. By iteratively solving the phonon Boltzmann transport equation, the κ_l can be readily obtained, as coded in the so-called ShengBTEprogram.[42] To ensure the convergence of the κ_l, a fine $21 \times 21 \times 21$ q-mesh is employed in the Brillouin zone.

3. Results and Discussion.

3.1. Structural Properties and Thermal Stability. As can be seen from Fig. 1, the β- and ε-GaSe possess hexagonal crystal structures with two unit layers (Se-Ga-Ga-Se), where the primitive cell contains eight atoms (four Ga and four Se). The β-GaSe with a space group of $P6_3/mmc$ [Fig. 1(a)] shows a stacking order of AA′, where the adjacent layers are rotated by 180° and stacked directly upon one another. In contrast, the ε-phase, with a space group of $P\bar{6}m2$ [Fig. 1(b)], is formed by a translation of the unit layer by 2/3 and 1/3 along the in-plane directions in alternating layers and exhibits an AB stacking order.[29] The calculated lattice constants of β-GaSe are $a = b = 3.804$ Å and $c = 16.10$ Å, while for the ε-GaSe they are $a = b = 3.806$ Å and $c = 16.05$ Å, which are in good agreement with those reported previously,[43–46] as summarized in Table 1. To check the thermal stability of both systems, we employ the *ab initio* molecular dynamics (AIMD) simulations carried out at 700 K for 10000 steps with a time step of 1 fs. Figure 2 displays the nearest Ga-Se, Ga-Ga, and interlayer distances with respect to the AIMD step. For the β-GaSe, we see from Fig. 2(a) that the fluctuation of the Ga-Se(Ga) distance reaches a maximum of 7.8% (6.7%) around the equilibrium bond length of

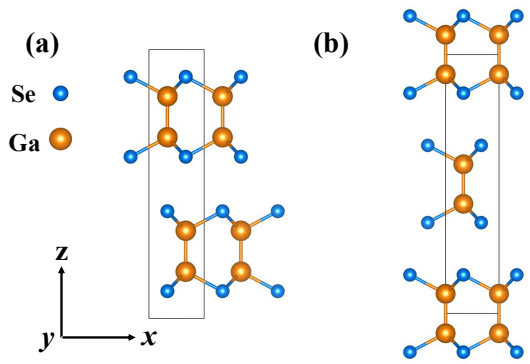

Fig. 1. The hexagonal crystal structures of the (a) β-GaSe and (b) ε-GaSe, which exhibit a space group of $P6_3/mmc$ and $P\bar{6}m2$, respectively.

Table 1. The lattice constants (in units of Å) of β- and ε-GaSe compounds. The previously reported theoretical and experimental results are also listed for comparison.

System	References	$a = b$	c
β-GaSe	This work	3.804	16.10
	Theory [45]	3.800	16.17
	Experiment [44]	3.755	15.955
ε-GaSe	This work	3.806	16.05
	Theory [46]	3.801	16.04
	Experiment [43]	3.755	15.949

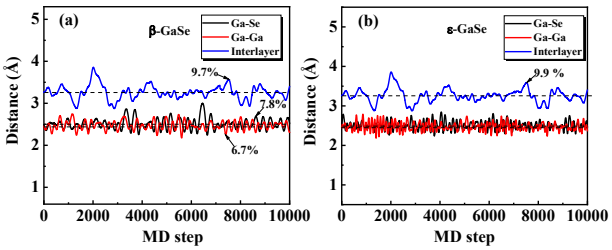

Fig. 2. The AIMD simulation results of various bonding distances in the (a) β-GaSe and (b) ε-GaSe at 700 K. The black dashed lines represent the corresponding equilibrium bond length. The maximum fluctuations of bonding or interlayer distances are marked by small arrows.

2.488 Å (2.449 Å) at 8632 (7383) AIMD step. In contrast, the interlayer distance exhibits a larger fluctuation, reaching 9.7% at 7527 step. A similar picture can be found for the ε-phase [Fig. 2(b)], where the maximum fluctuation of the interlayer distance reaches 9.9% at 7513 AIMD step. All these observations suggest that both structures are thermally stable at 700 K. Indeed, the single-crystalline β- and ε-GaSe have been successfully synthesized by using molecular beam epitaxy.[28]

3.2. Phonon Transport Properties. Figure 3(a) plots the phonon dispersion relations of β- and ε-GaSe, where there is no imaginary frequency, guaranteeing the dynamic stability of both structures. It is surprising to find that the two systems exhibit almost identical phonon dispersions, although they have distinct stacking patterns. If we focus on the low-frequency region ($0 \sim 20\,\mathrm{cm}^{-1}$), we detect that the ε-GaSe exhibits slightly lower phonon frequencies in comparison with β-GaSe, particularly along the Γ–A path, as indicated in Fig. 3(b). Such an observation can be attributed to the different structural symmetry of the two phases, which causes the atoms to vibrate in distinct phonon modes, as previously found in the α- and β-Ge_2Sb_2.[47]

Figure 3(c) shows the temperature dependence of the lattice thermal conductivities of the β- and ε-GaSe. It is obvious that both systems show strong anisotropy, and the κ_l along the z-direction is significantly smaller than that along the x (in-plane)-direction. This is reasonable since there exist stronger intralayer bonding but weaker interlayer vdW interactions in both structures. Interestingly, we find that the κ_l of ε-GaSe is much lower compared with that of the β-phase in either direction, although they exhibit similar phonon dispersions with each other. For example, the room-temperature κ_l of β- and ε-GaSe are found to be 6.32 (0.58) $\mathrm{W{\cdot}m^{-1}{\cdot}K^{-1}}$ and 3.61 (0.28) $\mathrm{W{\cdot}m^{-1}{\cdot}K^{-1}}$ along the $x(z)$-directions, respectively. Note that the lattice thermal conductivity can be expressed as $\kappa_l = \frac{1}{V}\sum_\lambda C_\lambda v_\lambda^2 \tau_\lambda$, where V, C, v, and τ are the volume of the primitive cell, the heat capacity, the group velocity, and the phonon relaxation time of phonon mode, respectively. Our calculation finds that the average group velocity v_λ ($0.724\,\mathrm{km{\cdot}s^{-1}}$) of β-GaSe almost coincides with that of ε-GaSe ($0.719\,\mathrm{km{\cdot}s^{-1}}$) due to their similar phonon dispersions [Fig. 3(b)]. In addition, we plot the phonon relaxation time τ_λ of the β- and ε-GaSe as a function of frequency, as shown in Fig. 4(a). It can be found that the τ_λ of ε-GaSe is distinctly lower compared with that of the β-GaSe, indicating strong anharmonic phonon scattering. Indeed, the average τ_λ values are calculated to be 5.21 ps and 3.46 ps for the β- and ε-phase, respectively. As known, the τ_λ is determined by the scattering phase space and lattice anharmonicity (characterized by the Grüneisen parameter γ). We see from Fig. 4(b) that

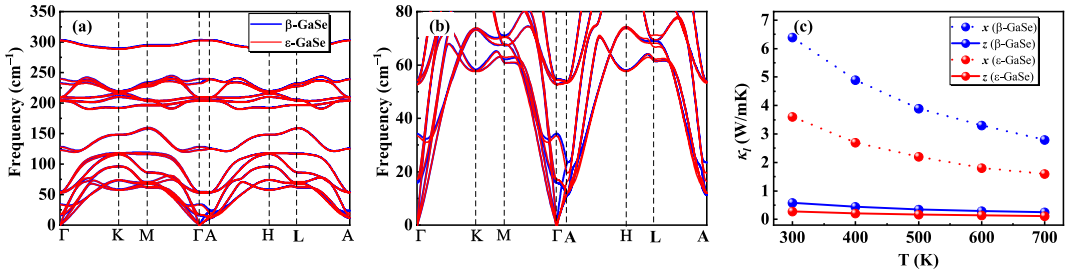

Fig. 3. (a) The phonon dispersion relations of β- and ε-GaSe. (b) The comparison of the phonon dispersions in the low-frequency region. (c) The lattice thermal conductivities plotted as a function of temperature along the x- and z-directions.

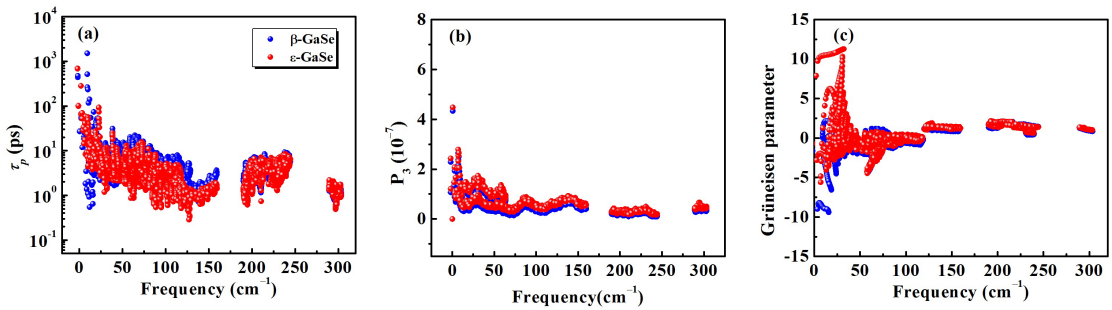

Fig. 4. (a) The phonon relaxation times, (b) the three-phonon scattering phase space, and (c) the Grüneisen parameter of the β- and ε-GaSe, plotted with respect to the phonon frequency. The obviously lower relaxation time of β-GaSe is mainly determined by its stronger lattice anharmonicity (characterized by the Grüneisen parameter).

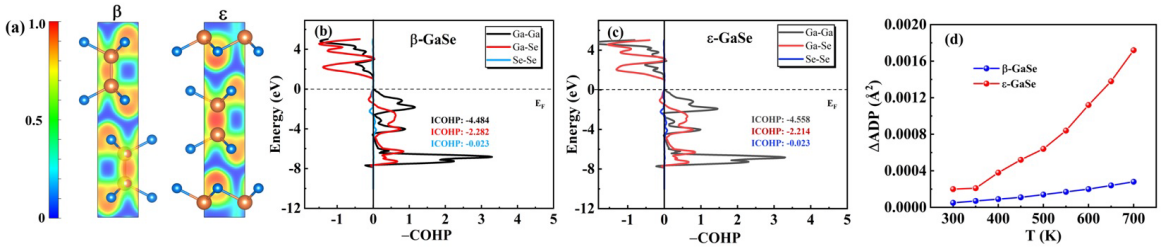

Fig. 5. The electronic localization function of (a) β- and ε-GaSe. (b) and (c) The corresponding crystal orbital Hamilton population (COHP) analysis of the nearest-neighbor atomic pairs. The ICOHP (bond strength by integrating the COHP of each bond up to the Fermi level, in units of eV) is also indicated. (d) The difference between the atomic displacement parameters of Ga and Se atoms for the β- and ε-GaSe, plotted as a function of temperature. All these comparisons demonstrate that the ε-GaSe possesses larger lattice anharmonicity.

the three-phonon scattering phase space P_3 of the ε-GaSe is comparable to that of the β-GaSe in a wide frequency range. However, the absolute γ value of the ε-GaSe is obviously larger than that of the β-GaSe, especially for the low-frequency region ($0 \sim 50\,\mathrm{cm}^{-1}$), as indicated in Fig. 4(c). Indeed, our calculations find that the average Grüneisen parameter is 1.85 and 1.66 for the ε-GaSe and β-GaSe, respectively. The larger γ value suggests strong lattice anharmonicity and thus lower thermal conductivity of the ε-GaSe. In principle, the bonding characteristic plays an important role in governing the phonon transport.

Figure 5(a) plots the electron localization function of the β- and ε-GaSe compounds. We observe a significant localization of electrons between the Ga and Se (Ga) atoms for both systems, suggesting strong covalent bonding between the neighboring atoms. To have a quantitative understanding of the bonding characteristics, we calculate the so-called crystal orbital Hamilton population (COHP) of the β- and ε-GaSe.[48–50] It should be noted that the positive and negative COHP respectively correspond to bonding and antibonding states, and the integrated COHP (ICOHP) reflects bond strength by integrating the COHP of each bond up to the Fermi level. Figures 5(b) and 5(c) show the COHP of various nearest-neighbor atomic pairs for the β- and ε-GaSe, respectively. If we focus on the standard deviation (Δ) of the ICOHP values, we find that the ε-GaSe has a larger Δ (1.852 eV) compared with that of the β-phase (1.821 eV). In other words, the ε-phase exhibits relatively stronger bonding heterogeneity, which further confirms the larger anharmonicity. To gain a deep insight into the underlying physical mechanism, we plot in Fig. 5(d) the atomic displacement parameter (ADP) difference ($\Delta\mathrm{ADP} = \mathrm{ADP_{Ga}} - \mathrm{ADP_{Se}}$) between the Ga and Se atoms for both the β- and ε-GaSe. We observe that the ΔADP of the ε-GaSe is obviously larger than that of the β-phase, which can be attributed to the stronger bonding heterogeneity in the ε-phase discussed above. Collectively, all these findings demonstrate that the ε-GaSe possesses larger lattice anharmonicity and thus smaller lattice thermal conductivity.

3.3. Electronic Transport Properties. Figures 6(a) and 6(b) plot the electronic band structures of the β- and ε-GaSe, respectively. We find that the band structures of the two phases are similar to each other. In particular, both systems show semiconducting behavior characterized by the conduction band minimum (CBM) and valence band maximum (VBM) located at the Γ point in the Brillouin zone. Moreover, the band gaps of the β- and ε-phases are respectively calculated to be 0.75 eV and 0.70 eV, which are in good agreement with previously reported results.[30,31] Notably, the energy bands around the VBM are doubly degenerate and exhibit weaker dispersions compared with those near the CBM, suggesting a larger effective mass of the p-type system. Indeed, the density of states (DOS) effective mass of holes (electrons) for the β- and ε-GaSe are calculated to be 0.907 (0.227)m_e and 0.894 (0.228)m_e, respectively. As the Seebeck coefficient is positively correlated with the effective mass governed by the Mott relation $S = \frac{8\pi^2 k_\mathrm{B}^2 T}{3eh^2} m^* \left(\frac{\pi}{3n}\right)^{2/3}$,[51] it is reasonable to expect that the p-type S value is larger than that of the n-type system at the same carrier concentration, which holds for both the β- and ε-GaSe and will be discussed later. Figure 6(c) shows the carrier relaxation time (τ) with respect to hole carrier concentration at 300 K. We see that the results of the β- and ε-phases are almost identical to each other due to their similar band structures. On the other hand, we observe that the relaxation time is dependent on crystal orientations[52] and the values along the z-direction are obviously lower than those along the x-direction. Such a finding could be attributed to the fact that the interlayer electron transport is limited due to the existence of weak vdW interactions, thus leading to a short out-of-plane relaxation time.

By solving the Boltzmann transport equation, the electronic transport coefficients (S, σ, and κ_e) of the GaSe can be readily evaluated, as shown in Fig. 7 (ε-phase) and Fig. S1 of the Supplementary Materials (SM) (β-phase) at 300 K. Interestingly, we find that the two systems exhibit almost identical transport coefficients. For simplicity, we focus only on the ε-phase in the following discussions. Figure 7(a) plots the Seebeck coefficient (absolute value) as a function of carrier concentration, where the S value decreases with increasing concentration, as is well-known to the TE community. Besides, we find that the p-type system exhibits a higher S compared with the n-type counterpart, primarily owing to the larger DOS effective mass of the hole, as mentioned above. In addition, we see that the p-type S shows weak anisotropy. For example, at a typical hole carrier concentration of $1 \times 10^{19}\,\mathrm{cm}^{-3}$, the S value can reach $257\,\mu\mathrm{V{\cdot}K}^{-1}$ and $229\,\mu\mathrm{V{\cdot}K}^{-1}$ along the x- and z-directions, respectively. Such a result should be attributed to the anisotropic effective masses of charge carriers. Indeed, our calculations suggest that the hole effective

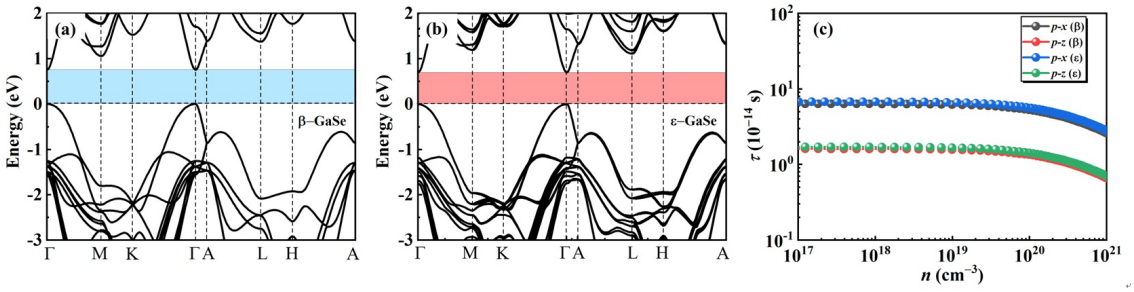

Fig. 6. The DFT calculated electronic band structure of (a) β-GaSe and (b) ε-GaSe. The colored areas indicate the corresponding band gap. (c) The relaxation time of holes as a function of carrier concentration at 300 K, where the results along the x- and z-directions are both shown.

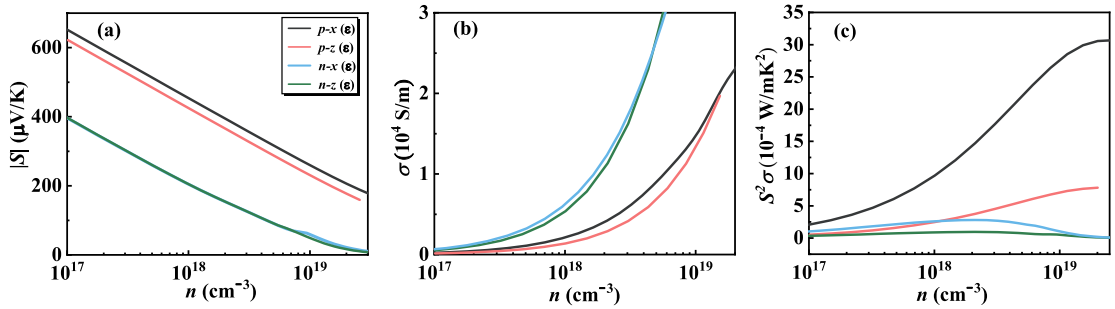

Fig. 7. (a) The calculated Seebeck coefficient, (b) the electrical conductivity, and (c) the power factor of ε-GaSe, plotted as a function of carrier concentration along the x- and z-directions at 300 K. The results for the p- and n-type are both shown.

mass ($1.212m_e$) along the x-direction is much larger than that along the z-direction ($0.121m_e$), which leads to higher intralayer S. On the other hand, we see from Fig. 7(b) that the electrical conductivity increases with carrier concentration and also exhibits direction dependence, especially for the p-type system where the in-plane σ is obviously larger than that of the out-of-plane, as determined by stronger intralayer covalent bonding. Besides, the σ of the n-type system is much larger than that of the p-type, which can be ascribed to the obviously lower DOS effective mass of the electron discussed above. As the electronic thermal conductivity is inherently connected with the electrical conductivity by the well-known Wiedemann–Franz law ($\kappa_e = L\sigma T$, where L is the Lorenz number), the carrier concentration dependence of κ_e is basically the same as that of σ, and we do not show it here.

Considering the inverse variations of the Seebeck coefficient and the electrical conductivity with respect to the carrier concentration, optimal power factors can be expected at moderate carrier concentration, as shown in Fig. 7(c). As the Seebeck coefficient dominates the contribution to the power factor, we observe significantly larger p-type value. For example, a maximum PF of $3.06 \times 10^{-3}\,\mathrm{W{\cdot}m^{-1}{\cdot}K^{-2}}$ ($0.28 \times 10^{-3}\,\mathrm{W{\cdot}m^{-1}{\cdot}K^{-2}}$) can be realized at hole (electron) carrier concentration of $2.57 \times 10^{19}\,\mathrm{cm^{-3}}$ ($2.09 \times 10^{18}\,\mathrm{cm^{-3}}$) along the x-direction. It is thus worth believing that the p-type system should exhibit better thermoelectric performance, which is thus the focus of our subsequent discussion.

To discuss the temperature dependence of electronic transport coefficients, we show the S, σ, and $S^2\sigma$ of p-type ε-GaSe along both the x- and z-directions in Fig. S2 of the SM. We see that the absolute S increases with the temperature, which is reasonable since it is proportional to temperature according to the Mott relation mentioned above. In contrast, the σ decreases with increasing temperature, and a similar behavior is observed in the carrier mobility μ [see the insets in Figs. S2(c) and S2(d) of the SM]. This is reasonable since μ is connected with σ by the relation $\sigma = ne\mu$. By combining the Seebeck coefficient and the electrical conductivity, the temperature-dependent power factors of the system are obtained, as illustrated in Figs. S2(e) and S2(f). As the temperature increases, the maximum power factor exhibits a slight increase followed by a slow decrease, with a peak value occurring at 400 K.

3.4. Figure of Merit. With all the electronic and phonon transport coefficients calculated, we are now able to evaluate the TE performance of β- and ε-GaSe. Figures 8(a) and 8(b) illustrate the temperature-dependent p-type ZT values along the x- and z-directions, respectively. Given that the power factor shows minimal variation with temperature, we see that the ZT values increase monotonically for both systems in the temperature range from 300 K to 700 K, as governed by the temperature dependence of lattice thermal conductivity shown in Fig. 3(c). We do not consider higher temperatures since both the β- and ε-GaSe compounds are thermally stable up to 700 K according to our AIMD simulations (Fig. 2). Interestingly, although the electronic transport coefficients of β- and ε-phase are almost identical to each other, the ZT values of ε-GaSe are obviously larger than those of the β-phase.

Table 2. The optimized ZT values and the corresponding transport coefficients of the β- and ε-GaSe along the x- and z-directions at 700 K.

System	Direction	n (10^{19} cm^{-3})	S (μV·K^{-1})	σ (10^4 S·m^{-1})	$S^2\sigma$ (10^{-4} W·m^{-1}·K^{-2})	$\kappa_l + \kappa_e$ (W·m^{-1}·K^{-1})	ZT
β-GaSe	z	2.95	244	1.08	6.50	$0.25 + 0.10$	1.3
ε-GaSe	z	1.76	285	0.69	5.63	$0.12 + 0.07$	2.1
β-GaSe	x	4.42	212	6.21	27.8	$2.80 + 0.61$	0.6
ε-GaSe	x	3.59	227	5.27	27.2	$1.60 + 0.52$	0.9

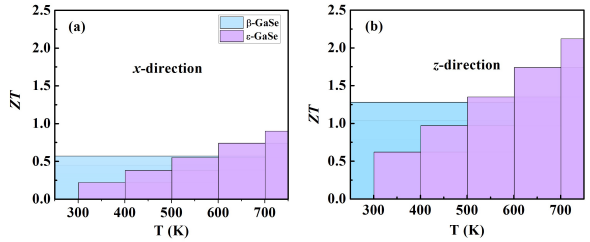

Fig. 8. The p-type ZT values of (a) β- and (b) ε-GaSe, plotted as a function of temperature along the x- and z-directions.

In particular, at an elevated temperature of 700 K, a maximum ZT of 1.3 (2.1) can be realized for the β (ε)-GaSe along the z-direction.

To have a better understanding of such different TE performance, Table 2 summarizes the optimized ZT values and their corresponding transport coefficients. It is found that the power factors of β- and ε-phase are indeed close to each other, especially for the in-plane values. Although the PF values along the z-direction are obviously lower, the total thermal conductivities ($\kappa_l + \kappa_e$) along the z-direction are even smaller, especially for the ε-phase, thereby leading to a much higher ZT value. Our results therefore indicate that the layered β- and ε-GaSe are very promising TE candidates, and appropriate p-type doping should be introduced to realize optimized carrier concentrations of 2.95×10^{19} cm^{-3} and 1.76×10^{19} cm^{-3}.

4. Conclusions. In summary, we have explored the structural, electronic, phonon, and thermoelectric transport properties of the β- and ε-GaSe compounds by combining DFT calculations with Boltzmann transport theory for both electrons and phonons. It is found that the two systems are dynamically and thermally stable with similar electronic transport coefficients and phonon dispersions. Nevertheless, the lattice thermal conductivities of these two phases are quite different from each other, which is essentially connected to the associated bonding heterogeneity. Collectively, the ε-GaSe exhibits better TE performance compared with the β-phase, and the intriguing anisotropic ZT values are found, which also highlights the promising material design strategy to decouple the transport coefficients and thus significantly enhance the energy conversion efficiency. Considering the fact that the single-crystalline β- and ε-GaSe have been successfully synthesized,[28] it is highly possible to realize their good TE performance by appropriate p-type doping.

Acknowledgements. This work was supported by the National Natural Science Foundation of China (Grant Nos. 62074114 and 12474019). The numerical calculations in this work have been done on the platform in the Supercomputing Center of Wuhan University.

References

[1] Pei Y Z, Shi X Y, LaLonde A, Wang H, Chen L D, and Snyder G J 2011 *Nature* **473** 66
[2] Pei Y Z, Wang H, and Snyder G J 2012 *Adv. Mater.* **24** 6125
[3] Liu W, Tan X J, Yin K, Liu H J, Tang X F, Shi J, Zhang Q J, and Uher C 2012 *Phys. Rev. Lett.* **108** 166601
[4] Biswas K, He J Q, Blum I D, Wu C I, Hogan T P, Seidman D N, Dravid V P, and Kanatzidis M G 2012 *Nature* **489** 414
[5] Jiang B B, Yu Y, Cui J, Liu X X, Xie L, Liao J C, Zhang Q H, Huang Y, Ning S C, Jia B H *et al.* 2021 *Science* **371** 830
[6] Zhou Y M and Zhao L D 2017 *Adv. Mater.* **29** 1702676
[7] Wu J, Chen Y B, Wu J Q, and Hippalgaonkar K 2018 *Adv. Electron. Mater.* **4** 1800248
[8] Stark M S, Kuntz K L, Martens S J, and Warren S C 2019 *Adv. Mater.* **31** 1808213
[9] Samanta M, Ghosh T, Chandra S, and Biswas K 2020 *J. Mater. Chem. A* **8** 12226
[10] Qin B C, Wang D Y, Liu X X, Qin Y X, Dong J F, Luo J F, Li J W, Liu W, Tan G J, Tang X F, Li J F, He J Q, and Zhao L D 2021 *Science* **373** 556
[11] Zhou J Y, Lin Z Y, Ren H Y, Duan X D, Shakir I, Huang Y, and Duan X F 2021 *Adv. Mater.* **33** 2004557
[12] Zhao L D, Tan G J, Hao S Q, He J Q, Pei Y L, Chi H, Wang H, Gong S K, Xu H B, Dravid V P *et al.* 2016 *Science* **351** 141
[13] Samanta M, Pal K, Pal P, Waghmare U V, and Biswas K 2018 *J. Am. Chem. Soc.* **140** 5866
[14] Wang C and Chen Y 2020 *npj Comput. Mater.* **6** 26
[15] Liu G, Lv Y Y, Jiang Z W, Liu G Z, Zhou X L, Zhang Y, Zheng J H, Xu L, Lu M H, Yao S H, Chen Y B, Zhou J, Xi X X, and Chen Y F 2024 *Phys. Rev. B* **109** 024302
[16] Carle M, Pierrat P, Lahalle-Gravier C, Scherrer S, and Scherrer H 1995 *J. Phys. Chem. Solids* **56** 201
[17] Xu P P, Fu T Z, Xin J Z, Liu Y T, Ying P J, Zhao X B, Pan H G, and Zhu T J 2017 *Sci. Bull.* **62** 1663
[18] Zhao L D, Lo S H, Zhang Y S, Sun H, Tan G J, Uher C, Wolverton C, Dravid V P, and Kanatzidis M G 2014 *Nature* **508** 373
[19] Chang C, Wu M H, He D S, Pei Y L, Wu C F, Wu X F, Yu H L, Zhu F Y, Wang K D, Chen Y, Huang L, Li J F, He J Q, and Zhao L D 2018 *Science* **360** 778
[20] Wang S F, Zhang Z G, Wang B T, Zhang J R, and Wang F W 2021 *Chin. Phys. Lett.* **38** 046301
[21] Li A R, Hu C L, He B, Yao M Y, Fu C G, Wang Y C, Zhao X B, Felser C, and Zhu T J 2021 *Nat. Commun.* **12** 5408
[22] Yagmurcukardes M, Senger R T, Peeters F M, and Sahin H 2016 *Phys. Rev. B* **94** 245407
[23] Jia T H, Fuh H R, Chen D Y *et al.* 2018 *Adv. Electron. Mater.* **4** 1700447
[24] Nitta H, Yonezawa T, Fleurence A, Yamada-Takamura Y, and Ozaki T 2020 *Phys. Rev. B* **102** 235407

[25] Zheng Y L, Li L, Li F F, Zhou Q, and Cui T 2020 *Chin. Phys. Lett.* **37** 088201
[26] Sorifi S, Aggarwal P, Kaushik S, and Singh R 2023 *ACS Appl. Electron. Mater.* **5** 451
[27] Dai Z R, Chegwidden S R, Rumaner L E, and Ohuchi F S 1999 *J. Appl. Phys.* **85** 2603
[28] Lee C H, Krishnamoorthy S, O'Hara D J, Brenner M R, Johnson J M, Jamison J S *et al.* 2017 *J. Appl. Phys.* **121** 094302
[29] Grzonka J, Claro M S, Molina-Sánchez A, Sadewasser S, and Ferreira P J 2021 *Adv. Funct. Mater.* **31** 2104965
[30] Al-Hattab M, Moudou L, Khenfouch M, Bajjou O, and Rahmani K 2022 *J. Nanopart. Res.* **24** 219
[31] Magorrian SJ, Zolyomi V, and Drummond N D 2021 *Phys. Rev. B* **103** 094118
[32] Nissimagoudar A S, Rashid Z, Ma J L, and Li W 2020 *Inorg. Chem.* **59** 14899
[33] Kresse G and Furthmuller J 1996 *Phys. Rev. B* **54** 11169
[34] Perdew J P, Burke K, and Ernzerhof M 1996 *Phys. Rev. Lett.* **77** 3865
[35] Kerber T, Sierka M, and Sauer J 2008 *J. Comput. Chem.* **29** 2088
[36] Madsen G K H and Singh D J 2006 *Comput. Phys. Commun.* **175** 67
[37] Li X, Zhang Z, Xi J Y, Singh D J, Sheng Y, Yang J, and Zhang W Q 2021 *Comp. Mater. Sci.* **186** 110074
[38] Ji J L, Tang Q H, Yao M J, Yang H L, Jin Y Q, Zhang Y B, Xi J Y, Singh D J, Yang J, and Zhang W Q 2022 *J. Am. Chem. Soc.* **144** 18552
[39] Wei B, Li J L, Yang Y Y, Li W, Zhou Z F, Zheng Y P, Zhang W Y, Chai Y F, Chang Z, Nan C W, and Lin Y H 2023 *npj Comput. Mater.* **9** 160
[40] Wan D, Bai S L, Li X D, Zhang J Y, Ai P, Guo W R, and Tang S W 2024 *J. Materiomics* **10** 1004
[41] Togo A and Tanaka I 2015 *Scripta Mater.* **108** 1
[42] Li W, Carrete J, Katcho N A, and Mingo N 2014 *Comput. Phys. Commun.* **185** 1747
[43] Kuhn A and Chevy A 1975 *Status Solidi* **31** 469
[44] Whitehouse C R and Balchin A A 1978 *J. Mater. Sci.* **13** 2394
[45] Rak Z, Mahanti S D, Mandal K C, and Fernelius N C 2009 *J. Phys. Chem. Solids* **70** 344
[46] Dien V K, Tien N T, Khanh N D, Han N T N, and Lin M F 2023 *Phys. Rev. B* **108** 205150
[47] Lou A, Liu Q B, and Fu H H 2022 *Phys. Rev. B* **105** 075431
[48] Maintz S, Deringer V L, Tchougréeff A L, and Dronskowski R 2013 *J. Comput. Chem.* **34** 2557
[49] Maintz S, Deringer V L, Tchougréeff A L, and Dronskowski R 2016 *J. Comput. Chem.* **37** 1030
[50] Steinberg S and Dronskowski R 2018 *Crystals.* **8** 225
[51] Heremans J P, Jovovic V, Toberer E S, Saramat A, Kurosaki K, Charoenphakdee A, Yamanaka S, and Snyder G J 2008 *Science* **321** 554
[52] Wang N, Li M, Xiao H, Zu X, and Qiao L 2020 *Phys. Rev. Appl.* **13** 024038